Nanoscale Advances

ROYAL SOCIETY OF CHEMISTRY

PAPER

View Article Online
View Journal | View Issue

Cite this: *Nanoscale Adv.*, 2025, **7**, 601

Study on the therapeutic effect and some immune factors by methotrexate modified superparamagnetic nanoparticles in rat mammary tumors†

Li Huang, ‡[a] Xing Zhao,‡[b] Jun Zhang,‡[c] Jiquan Zhang, [d] Weike Liao,[d] Yanhua Fan,[d] Jintian Tang,*[e] Zhixu He,[b] Fuping Gao[e] and Weiwei Ouyang*[a]

Objective: this study investigates the efficacy, immunological impact, and preliminary safety of methotrexate (MTX) modified magnetic Fe_3O_4 nanoparticles in thermochemotherapy for mammary tumors in rats. *Methods*: transmission electron microscopy images revealed that the MTX-modified magnetic Fe_3O_4 nanoparticles are nearly spherical, approximately 10 nm in diameter. Chemically co-precipitated PEI-modified magnetic nanoparticles were utilized for thermotherapy, while MTX-modified nanoparticles were employed for thermochemotherapy. These nanoparticles were locally injected into the Walker-256 tumor tissues of Wistar rats. The experimental design included twelve groups, encompassing various protocols of thermotherapy and thermochemotherapy at 47 °C and 42 °C, a group receiving only MTX nanoparticle chemotherapy, and several control groups. The biodistribution of residual magnetic nanoparticles was assessed in vital organs such as the heart, liver, lungs, kidneys, and brain. *Results*: demonstrated that these magnetic nanoparticles primarily accumulated in the tumor's central region and were unevenly distributed at the margins. The nanoparticles were capable of penetrating tumor cells but were more dispersed around them. Importantly, no residual magnetic nanoparticles were detected in vital organs. Significant tumor reduction and prolonged survival times were observed in the 47 °C thermochemotherapy group, the 47 °C thermotherapy group and the repeated 42 °C thermochemotherapy group. Additionally, significant increases in IL-2 and IFN-γ levels, along with a decrease in IL-4 levels, were detected in the 47 °C thermochemotherapy and 47 °C thermotherapy groups. *Conclusion*: MTX-modified Fe_3O_4 magnetic nanoparticles demonstrate potential as an effective medium for thermochemotherapy. They are safe, tolerable, contribute to prolonged survival, and enhance immune functions in tumor-bearing rats without leaving residues in vital organs. These results provide a promising foundation for future cancer treatment research.

Received 7th April 2024
Accepted 18th November 2024

DOI: 10.1039/d4na00295d

rsc.li/nanoscale-advances

1. Introduction

Thermotherapy has emerged as another significant cancer treatment following surgery, radiotherapy, chemotherapy, and biological immunotherapy. The combination of thermotherapy and chemotherapy is regarded as an effective comprehensive cancer treatment mode.[1] However, chemotherapy drugs are known for their severe toxicity and side effects, along with a clear dose-effect relationship. Thus, to enhance local drug concentration and reduce systemic toxicity and side effects, the targeted route of administration is being considered. With the advancement of nanotechnology, it has been discovered that the chemical composition, size, shape, morphology, and magnetic behavior of nanoparticles are the most critical indicators determining their biomedical application.[2] Based on these findings, nanoparticles can be used for early detection and visualization of cancer development, and can be used for

[a]*Department of Thoracic Oncology, The Affiliated Hospital of Guizhou Medical University and the Affiliated of Cancer Hospital of Guizhou Medical University, Guiyang, 550004, China. E-mail: ouyangww103173@163.com*

[b]*Stem Cell and Tissue Engineering Research Center, Guizhou Medical University, Guiyang, 550004, China*

[c]*Department of Pathology, The Affiliated Hospital of Guizhou Medical University and The Affiliated of Cancer Hospital of Guizhou Medical University, Guiyang, 550004, China*

[d]*Guizhou Provincial Engineering Technology Research Center for Chemical Drug R&D, Guizhou Medical University, Guiyang, 550004, China*

[e]*Key Laboratory of Particle and Radiation Imaging, Ministry of Education, Institute of Medical Physics and Engineering, Department of Engineering Physics, Tsinghua University, Beijing, 100083, China. E-mail: tangjt@mail.tsinghua.edu.cn*

† Electronic supplementary information (ESI) available. See DOI: https://doi.org/10.1039/d4na00295d

‡ These authors have contributed equally to this work.

diagnosis and treatment. Nanoparticles are being designed as multifunctional vehicles to deliver anticancer agents, genes, or proteins directly to targeted tumors.[3–8]

Currently, most *in vivo* and *in vitro* experiments with ferrofluid hyperthermia employ local multidirectional injection and co-culture techniques. These methods, followed by the controlled manipulation of magnetic nanoparticles towards the direction of an externally applied magnetic field, have demonstrated significant anti-tumor effect.[1,3,9] At the same time, several studies have concluded that ferrofluid hyperthermia can reduce the radiotherapy dose and enhance the effect of chemotherapy.[2,3,9] Nanoparticles have been shown to stimulate immune cells to attack tumor cells.[3,10] In clinical trials for various cancers, including prostate, brain, liver, bone, and some metastatic cancers, ferrofluid has demonstrated effective targeting and improved efficacy.[11–14] Additionally, when ferrofluid carries chemotherapy drugs, it not only provides a hyperthermia effect but also ensures high sustained-release concentrations of local chemotherapy drugs with mild systemic toxicity and side effects.[3] Most current research on nanoparticle thermochemotherapy is still at the stage of fundamental theory and animal experimentation. However, some clinical trials have been conducted with nanoparticles carrying chemotherapeutic agents, such as lyso-thermosensitive liposomal doxorubicin (LTLD), which underwent a phase III clinical trial[8] for unresectable hepatocellular carcinoma (HCC) based on the results of a phase I trial.[15,16] The conclusion was that LTLD combined with radiofrequency ablation (RFA) is generally safe for the treatment of HCC, but no significant improvement in progression-free survival (PFS) or overall survival (OS) was observed compared to RFA alone. However, in the subgroup of patients with a single HCC lesion treated with RFA for more than 45 minutes, an improvement in OS was noted in the combined treatment group. Methotrexate (MTX), a folic acid analogue, acts as an anticancer agent and a specific targeting moiety that binds to the folate receptor on the cancer cells' surface, facilitating internalization through receptor-mediated endocytosis.[17,18] Based on the chemical reaction between MTX and superparamagnetic nanoparticles, a dual-targeted drug carrier has been designed. This carrier utilizes the conjugation of MTX and superparamagnetic nanoparticles to enhance tumor targeting efficiency and accumulation. The unique local specific distribution of MTX, *via* the folate receptor, and the directional controllability of superparamagnetic nanoparticles in a magnetic field, contribute to this enhancement.[18,19] In this study, MTX-modified magnetic nanoparticles (MTX-MNPs) were injected into tumor tissues to observe their therapeutic effect and impact on immune function, and to preliminarily evaluate their safety.

2. Materials and methods

2.1. Preparation and surface modification of magnetite nanoparticles

Magnetic Fe_3O_4 nanoparticles prepared by controlled chemical co-precipitation of Fe^{2+} and Fe^{3+} (1 : 2 of molar ratio). In a typical experiment, $FeCl_3 \cdot 6H_2O$ (11.6 g) and $FeCl_2 \cdot 4H_2O$ (4.30 g) were dissolved in 400 mL of deionized water under nitrogen gas protection with vigorous stirring at 85 °C. Subsequently, about 20 mL of 25 wt% ammonia solution was added to the solution and stirring continued for another 20 min to allow growth of the nanoparticles. The solution was then cooled to room temperature and the resulting particles were subjected to magnetic decantation followed by repeated washing with distilled water and ethanol. The resulting nanoparticles were further analyzed through the 8600 series vibrating sample magnetometer, and the magnetization curve was plotted to confirm their superparamagnetism. Additionally, Energy Dispersive X-ray Spectroscopy (EDX) and X-ray Photoelectron Spectroscopy (XPS) were used to verify whether the magnetite nanoparticles were successfully synthesized. The obtained superparamagnetic magnetite nanoparticles were first surface-modified with PEI to form a self-assembled monolaye and subsequently conjugated with MTX through amidation between the carboxylic acid end groups on MTX and the amine groups on the particle surface. 5 mL of a 20% PEI solution was added to a colloidal suspension of 20 mg of magnetite nanoparticles in 100 mL of distilled water to obtain PEI-modified magnetic nanoparticles (PEI-MNPs). The nanoparticles were sonicated in a sonicating bath for 4 h at 60 °C. The resulting aminated nanoparticles were then isolated using a rare earth magnet and washed twice with 200 mL proof ethanol and twice with deionized water. To conjugate the nanoparticles with MTX, free MTX (0.5 g), NHS (0.07 g), and EDC (0.097 g), were dissolved in PBS (20 mL). The pH of the solution was adjusted to 8 by addition of 1.0 M NaOH and the mixture was to react allow for 30 min in ambient temperature. The solution of MTX was then mixed with 100 mL of 20% colloidal suspension of magnetite nanoparticles. The resulting suspension was agitated overnight at 37 °C in the dark. Following MTX conjugation, the free MTX was removed by ultracentrifugation (Hitachi, CF 16RX) at 15 000 rpm for 20 min at 4 °C and ultracentrifugation was repeated three times. All supernatants were collected and the amount of MTX was determined by JASCO UV/Vis 570 at 304 nm.

2.2. Characterization and temperature monitoring of magnetic nanoparticles modified with methotrexate

The morphology of MTX-MNPs characterized by a Tecnai TF20 transmission electron microscope (TEM). The operation voltage was kept at 80 kV. TEM samples were prepared by deposition of a diluted particle suspension (5 μL) onto a carbon-coated copper grid and air-dried before the measurement. The average size, size distribution, and zeta potential changes of MTX-MNPs were determined by Dynamic Light Scattering (DLS) (Malvern Mastersizer 3000) in deionized water, which simultaneously confirmed their stability. The surface potential of functionalized Fe_3O_4 nanoparticles was measured by a Malvern Zetasizer Nano ZS model ZEN3000 (Worcestershire, UK) equipped with a standard 633 nm laser. The heating properties of magnetic nanoparticles in an alternating magnetic field (AMF) were observed using a heating system of the Magnetic Induction Therapy Device (MIH-100/170) designed by Tsinghua University. The device operates with a power supply voltage of 380 V

and a power supply frequency of 50 Hz. The magnetic field frequency ranges from 100 to 400 kHz, with a magnetic induction intensity of 40 to 170 Gs. The temperature was monitored using a thermocouple (It-18 copper-constantan thermocouple manufactured by Physitemp, 1 mm diameter and 0.1 s temperature response time) in an AMF (frequency: 300 kHz, field intensity: 130 Gs).

2.3. Experimental animal grouping

240 female Wistar rats, weighting about 100 g, were provided by the Laboratory Animal Center of the Chinese Academy of Medical Sciences. All animal procedures were performed in accordance with the Guidelines for Care and Use of Laboratory Animals of Guizhou Medical University and approved by the Animal Ethics Committee of Guizhou Medical University. The Walker-256 tumor cell line was purchased from the Institute of Materia Medica, Chinese Academy of Medical Sciences and Peking Union Medical College. Ten rats were no inoculation Walker-256 tumor cell lines as the normal group (normal). The Walker-256 tumor cell suspension (1×10^7 mL^{-1}, 0.2 mL) was subcutaneously injected into mammary glands of the right anterior part of chest in 230 rats. Seven days later, a size of 1.5 cm–2.0 cm tumor was grown in 194 rats. Three anesthetic death rats were excluded, the remaining 191 rats were randomly divided into 11 groups for entering into the experiment: 47TC (47 °C thermochemotherapy for 30 min): 24 rats inoculated with magnetic fluid (water-based magnetic fluid, superparamagnetic, diameter of about 10 nm, made by Key Laboratory of Particle & Radiation Imaging, Ministry of Education, Institute of Medical Physics and Engineering, Department of Engineering Physics, Tsinghua University) containing MTX 5.7 mg mL^{-1} were raised to 47 °C in AMF for 30 min; 47T (47 °C thermotherapy for 30 min): 24 rats inoculated with magnetic fluid modified by PEI were raised to 47 °C for 30 min; 42 TC (42 °C thermochemotherapy for 60 min): 21 rats inoculated with magnetic fluid containing MTX were raised to 42 °C for 60 min; 42T (42 °C thermotherapy for 60 min): 21 rats inoculated with magnetic fluid modified by PEI were raised to 42 °C for 60 min; repeated 42TC (repeated 42 °C thermochemotherapy for 60 min): 12 rats injected with magnetic fluid containing MTX were heated to 42 °C for 60 min; 2–5 fraction, interval of 72 h; repeated 42T (repeated 42 °C thermotherapy for 60 min): 12 rats injected with PEI modified magnetic fluid were heated to 42 °C for 60 min, 2–5 fraction, interval of 72 h; magnetic fluid chemotherapy group (MFC): 16 rats injected with magnetic fluid containing MTX were without being put into an AMF, two rats were sacrificed at 24 h after treatment for the pathological examination; control group (C): 21 rats inoculated with tumor and without any other treatment; magnetic field control group (M): 12 rats were put into an AMF for 30 min; magnetic fluid control group (MF): 12 rats injected with PEI modified magnetic fluid without put into an AMF; MTX chemotherapeutics group (MTX): 16 rats were administered 20 mg kg^{-1} (ref. 20) of MTX chemotherapy drug into the tumor, two rats were sacrificed at 24 h after treatment for the pathological examination (Table S1†). Two rats of each group were immediately euthanized using pentobarbital sodium anesthesia for the pathological examination after treatment, except for the normal group, MFC, MTX group. Two rats at 12 h and three at 24 h after treatment of each group in the 47TC, 47T, 42TC, 42T and C sacrificed for pathological examination and electron microscopic examination at 24 h. Four rats of each group in 47TC, 47T, 42TC, 42T, MFC, MTX, C and normal were sacrificed at the fourteen days after treatment and the peripheral blood was collected to measure the levels of IL-2, IFN-γ, and IL-4, and the remaining rats were observed for the long-term survival.

2.4. Magnetic fluid injection in the tumors

The rats with tumor were injected the magnetic fluid into the tumor at 24 h before hyperthermia to make magnetic nanoparticles more uniform distribution in the tumor tissues. In order to more effectively control the tumor tissues at the margins, to reduce the residual tumor tissues at the margins and the possibility of tumor recurrence and to increase control of subclinical lesions, the magnetic fluid was injected around the tumor margin. Firstly, the actual size of the tumor was measured. According to the literature of Hilger *et al.*[21] the tumor volume was calculated by using the formula $V = \pi/6 \times$ (product of three principal diameters), as described by steel. The total amount of injected magnetic fluids in the tumor for each rat was half of the tumor volume.[22] Based on six clockwise directions, the multi-point injection of magnetic fluids was conducted in the tumor tissue. 1 mL of magnetic fluid subcutaneously injected at six points of the tumor margins after 24 h, and heated into the alternating magnetic field 30 min after injection.

Before entering the AMF for heating, two rats from the 47 TC and repeated 42TC groups were randomly selected for X-ray imaging to assess the distribution of the magnetic fluids in and around the tumor. At 2 weeks post-treatment, two rats from the 47TC and 47T groups were randomly selected for X-ray imaging to evaluate the local distribution of the magnetic fluids. Similarly, at 2 months post-treatment, two rats from the 47T and repeated 42T groups were randomly selected for X-ray imaging.

2.5. Heating treatment in the alternating magnetic field

Six thermocouples connected to an eight-channel temperature indicator (XS01A-4, Beijing Kunlun Tianchen Instrument Science & Technology Co., Ltd) were used to monitor temperature changes in the tumor center, 0.5 cm outside of the tumor center, tumor edge, 0.5 cm and 1 cm outside of the tumor edge, and body temperature of rats (rectal temperature).

2.6. Pathological examination

The heart, liver, lung, kidney, and brain tissues were removed using the neutral formalin-fixed method, cutting a slice of 5 μm thick tissue along the maximum section of tissues to examine the residues of magnetic nanoparticles in the tissues using the Prussian blue staining.

2.7. Detection of IL-2, IFN-γ and IL-4 levels in the peripheral blood by ELISA

Fourteen days after treatment, four rats in each group of the 47TC, 47T, 42TC, 42T, MFC, C, MTX, and normal group sacrificed and peripheral blood was collected. Heparin was used to anticoagulate peripheral blood (1 mL), and density gradient centrifugation was used to centrifugate cytokines from 0.2 mL plasma. ELISA was used to measure the levels of IL-2, IFN-γ and IL-4 in 0.2 mL plasma (IL-2, IFN-γ and IL-4 kits were purchased from R&D System). An ELISA reader was used to measure the OD450 (Bio-Rad 680, Hercules, CA) for calculation of sample concentration.

2.8. Statistical analysis

Data analysis was performed using SPSS 16.0 software. For normally distributed data, results were presented as mean ± standard deviation, and multiple group comparisons were conducted using analysis of variance (ANOVA), with statistical significance set at $P < 0.05$. Fisher's exact test was used for analysis given the small sample size and few positive results, with statistical significance set at $P < 0.05$. Non-normally distributed data were presented as median and interquartile range (P_{25}, P_{75}), and multiple independent samples were compared using the Kruskal–Wallis H test, with statistical significance set at $P < 0.05$. Pairwise comparisons for the tumor volume and long-term survival in rats were conducted using the Mann–Whitney U test. Non-parametric tests were utilized to compare changes in tumor volume across pairwise comparisons among 11 groups. The significance level was adjusted to $0.05/11 = 0.0045$, with $P' < 0.0045$ considered statistically significant. Non-parametric tests were utilized to comparisons for long-term survival across pairwise comparisons among 12 groups. The significance level was adjusted to $0.05/12 = 0.004$, $P'' < 0.004$ considered statistically significant.

3. Results

3.1. Characterization and *in vitro* temperature measurement of magnetic nanoparticles modified with methotrexate

The detailed preparation of the MTX-MNPs is shown in experimental section. EDX revealed a uniform distribution of C, O and Fe in Fe_3O_4 nanoparticles (Fig. 1A). Zeta potential of synthesized Fe_3O_4 nanoparticles were negatively charged (zeta potential = −24.3 ± 2.6 mV). Along with PEI modification, the zeta potential of the nanoparticles significantly increased to a positive surface potential (zeta potential = 17.8 ± 1.8 mV) due to the positive charge of PEI (Fig. 1B). However, after conjugation of MTX, the zeta potential of the nanoparticles decreased (zeta potential = 3.63 ± 0.52 mV) due to the conjugation of the nanoparticle surface amine groups with MTX. Subsequently, XPS analysis also revealed the coexistence of C, N, O and Fe signals (Fig. 1C). More importantly, MTX-MNPs is superparamagnetic. All the above results confirmed the successful synthesis of MTX-MNPs.

TEM imaging was next used to show that the MTX-MNPs were nearly spherical in shape, with an approximate size of 10 nm (Fig. 1D). The mean diameter of these nanoparticles determined by DLS was 30.1 ± 5.2 nm (PDI = 0.23), which was larger than the size determined by TEM. The DLS experiment also demonstrated the colloidal stability of the particles in the aqueous phase through longitudinal studies (Fig. 1E), with no significant aggregation observed. The difference in the diameter of MTX-MNPs between TEM and DLS was mainly attributed to three factors. First, the sample preparation processes were different: TEM measured the size of the sample in the dried state, while DLS measured the size in the hydrated state. Second, the polymer shell on the surface of the particles tends to expand in aqueous media, which inevitably increases the size of the nanoparticles. Third, some particles may aggregate in the aqueous media. Fig. 1F shows the temperature change of 300 mg mL^{-1} concentrations of PEI-MNPs and MTX-MNPs in an AMF. The temperature of 300 mg mL^{-1} PEI-MNPs rises rapidly in the AMF and reaches 100 °C in 162 seconds, while the temperature of 300 mg mL^{-1} MTX-MNPs rises to 100 °C in 216 seconds. The calculated results indicate that the Specific Heat Absorption Rate (SAR) value of the PEI-MNPs suspension is approximately 6.45 W g^{-1}, and the Specific Lost Power (SLP) value is approximately 25 W g^{-1}. For the MTX-MNPs, the SAR value is approximately 4.84 W g^{-1}, and the SLP value is approximately 20 W g^{-1}. In the magnetization curve (Fig. S1†), the MNPs show typical superparamagnetic characteristics: the magnetization increases with the external magnetic field, and when the external field is removed, the magnetization drops almost immediately to zero without residual magnetization (*i.e.*, no hysteresis), indicating that these nanoparticles possess superparamagnetism. This characteristic is a hallmark of superparamagnetic materials, demonstrating that they have a reversible magnetization response under an external magnetic field with no persistent magnetism.

3.2. Temperature measurement and monitoring during treatment of tumor-bearing rats in the AMF

The tumor center temperature was controlled to reach the setting temperature (42 °C or 47 °C) in about 2 min. The temperature at 0.5 cm away from the tumor center was 1.5 °C–2 °C lower than in the tumor center, while the temperature of tumor edge was 2 °C–3 °C lower than in the tumor center. The temperature at 0.5 cm away from the tumor edge was slightly higher than at the tumor edge, and the temperature at 1 cm away from the tumor edge was slightly higher than the rectal temperature. The rectal temperature is between 36 °C ~37 °C.

3.3. Histological observation

3.3.1. General observation. The tumor volume in the C, M, MF, and MTX group was gradually increased with prolonged survival time, some rats showed a partial rupture of the tumor and tumor center liquefaction necrosis, tumor at the margins continued to grow. Some rats in the 47TC, 47T, repeated 42TC, and repeated 42T showed necrotic exfoliation and eschar on the surface of tumor after treatment. In the 47TC group, one rat showed completely exfoliated tumor, the wound surface showed dark brown magnetic nanoparticles and bleeding (Fig. 2A).

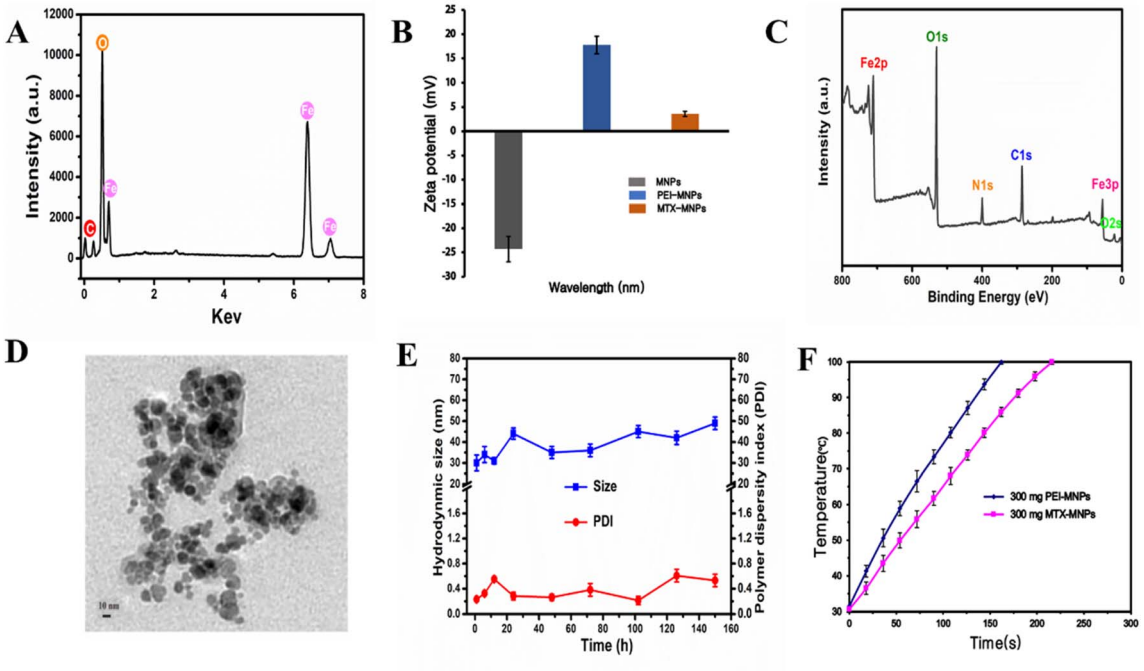

Fig. 1 Composition characterization and basic structure. (A) EDX spectral analysis indicating signals of C, O, and Fe in MNPs. (B) Zeta potential variation for MNPs, PEI-MNPs, and MTX-MNPs. (C) XPS spectra showing C, N, O, and Fe elements in MTX-MNPs. (D) TEM image of MTX-MNPs, scale bar is 10 nm. (E) Statistical graph showing the changes in particle size and PDI of MTX-MNPs over 150 hours. (F) Temperature variation of PEI-MNPs and MTX-MNPs in an AMF.

Eleven rats in the 47TC group had an exfoliated scab 2 to 3 weeks after treatment, and survived after the surface skin gradually healed. Six rats in the 47T group recovered at 2 to 3 weeks after treatment, and another one survived with tumor for 33 days, and recovered with the tumor gradual shrinking. Five rats in the repeated 42TC group and 3 rats in the repeated 42T group showed exfoliated tumor tissues with eschar and recovered at about 2–3 weeks after treatment. Two rats in the 42 TC group had a completely exfoliated tumor and recovered at about 18 days and 22 days after treatment, but one of them died at 74 days due to tumor recurrence. Residual magnetic nanoparticles were visible to the naked eye on the treated skin of 11 rats at 120 days after treatment (Fig. 2B). The heterogeneity of tumor growth can be seen in the MFC group. Two rats gradually

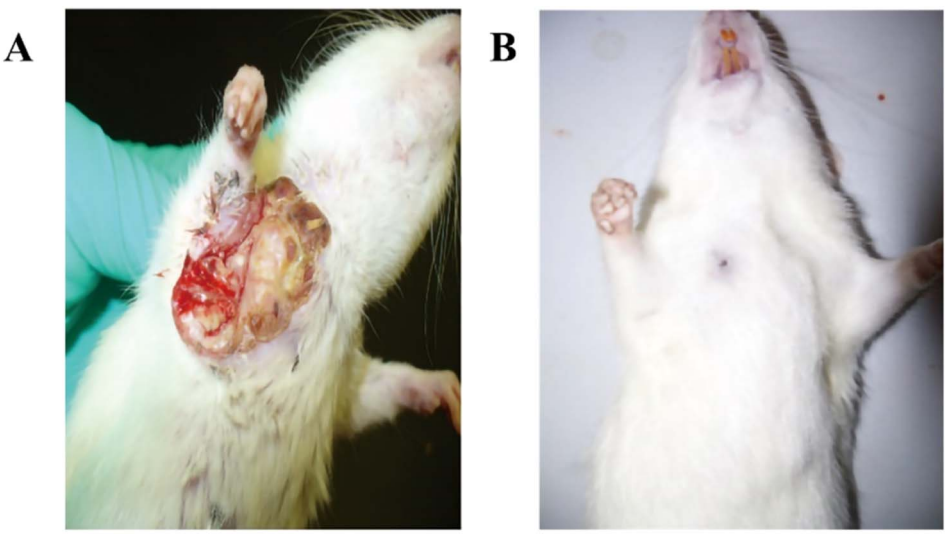

Fig. 2 General observation photograph in rats after hyperthermia and the distribution of magnetic nanoparticles in tumor tissue. (A) Tumor shedding, the wound showed a dark brown magnetic fluid and bleeding; (B) tumor shedding, local area showed residual magnetic nanoparticles at repeated 42TC.

reduced and complete remission of tumors can be seen at 22 days and 28 days after treatment, and the tumors of remaining rats gradually increased. No significant inhibition of MTX to tumor can be seen in the MTX group, and the tumor can grow rapidly. The tumor growth in the M and MF group was the same as in the C group.

3.3.2. Light microscope observation. At immediately, 12 hours and 24 hours post thermotherapy/thermochemotherapy, trace deposition of magnetic nanoparticles was observed in the meningeal microvasculature of a single rat in the 47T group at 24 hours (Fig. 3). Under optical microscopy at 400× magnification, no magnetic nanoparticle deposition was detected in the tissue structures of the heart, liver, lungs, kidneys, or brain parenchyma across all groups of rats. Based on the positive and negative detection results of magnetic nanoparticles across all examined organs, Fisher's exact test yielded $P = 0.167$. As $P > 0.05$, the result did not reach statistical significance.

3.3.3. Electron microscope observation. The images are magnified 4000 times under Electron Microscope. 24 h after 47T thermotherapy, PEI-MNPs entered into the cytoplasm, the wider distribution of magnetic nanoparticles among cells can be seen, with the cell membrane damage, cytoplasmic shrinkage, even bare nuclei (Fig. 4A). 24 h after 47TC thermochemotherapy, the wider distribution of MTX-MNPs around the cells can be seen, with the cell membrane damage, cytoplasmic shrinkage, and the vacuolar changes (Fig. 4B). 24 h after 42T thermotherapy, a large number of magnetic nanoparticles distributed around the tumor cell, and the cell was destroyed (Fig. 4C). 24 h after 42TC thermochemotherapy, the wider distribution of magnetic nanoparticles among cell can be seen, and the cell was destroyed, and the damaged cell had magnetic nanoparticles (Fig. 4D). Several tumor cells were visible in the field of view, with large nuclei and large nucleolus in group of C (Fig. 4E).

3.4. X-ray examination for different times after injection of magnetic fluid

After injection of magnetic fluid, the X-ray photograph showed a high-density shadow of the magnetic fluid, the evenly distributed magnetic nanoparticles at the tumor center, the unevenly distributed magnetic nanoparticles at the tumor margins, and continuously interrupted distributed magnetic nanoparticles around the tumor (Fig. 5A). At 2 weeks after treatment, the residual high-density shadow of magnetic nanoparticles can be seen at localized subcutaneous tissues under the X-ray, and the tumor tissue was significantly reduced (Fig. 5B). Two months after treatment, rats with visible magnetic nanoparticles residue with the skin was excluded, and there was no obvious residual high-density shadow of magnetic nanoparticles can be seen at the local subcutaneous tissue, and no local tumor in the rats (Fig. 5C).

3.5. Effect of treatment on tumor volume in rats

The tumor volumes were as follows before treatment: 47 TC group (2.71 ± 0.53) cm^3, 47T group (2.77 ± 0.29) cm^3, 42TC group (2.54 ± 0.60) cm^3, 42T group (2.52 ± 0.52) cm^3, repeated 42TC group (2.73 ± 0.37) cm^3, repeated 42T group (2.63 ± 0.42) cm^3, MFC group (2.59 ± 0.42) cm^3, C group (2.60 ± 0.59) cm^3, M group (2.53 ± 0.38) cm^3, MF group (2.59 ± 0.52) cm^3, and MTX group (2.59 ± 0.36) cm^3. There was no significant difference in tumor volume among the groups of rats before treatment. Two weeks post-treatment, tumor was disappeared in 2 rats of the 47TC group, 2 rats of the 47T group, and 1 rat of each of the 42TC and 42T groups. The tumor volumes were as follows: 47 TC group 0.60 (0.04, 6.17) cm^3, 47T group 1.69 (0.32, 8.48) cm^3, 42TC group 22.34 (1.91, 29.88) cm^3, 42T group 22.96 (20.10, 27.33) cm^3, repeated 42TC group 7.03 (0.06, 15.52) cm^3, repeated 42T group 4.58 (0.16, 7.77) cm^3, MFC group 26.71

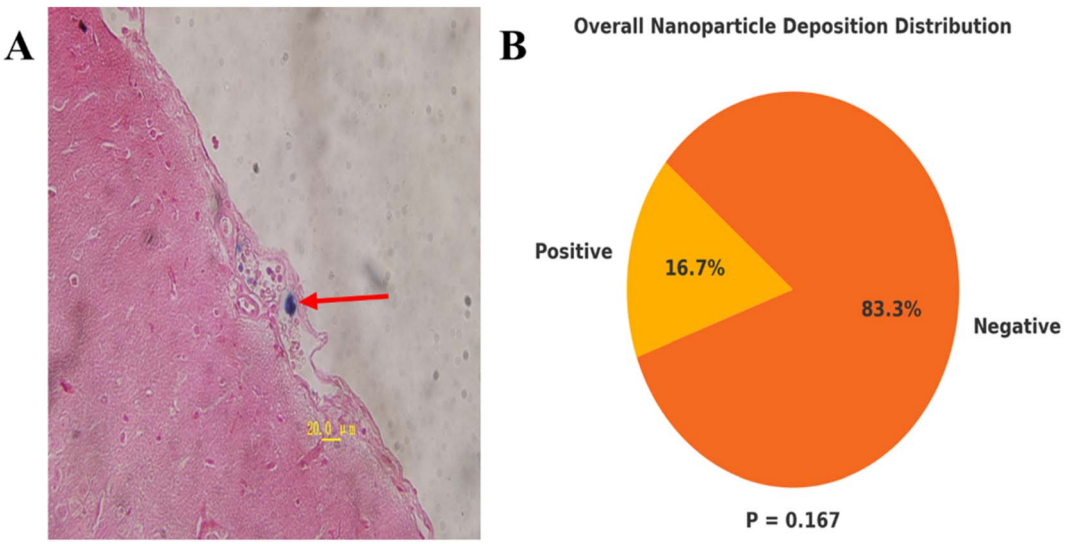

Fig. 3 Magnetic nanoparticle distribution in normal tissues and statistical analysis. (A) Magnetic nanoparticles found in the meningeal microvasculature (indicated by arrows stained with Prussian blue). Scale bar is 20 μm. (B) Overall statistical analysis of positive and negative results across all examined organs, with Fisher's exact test showing $P > 0.05$.

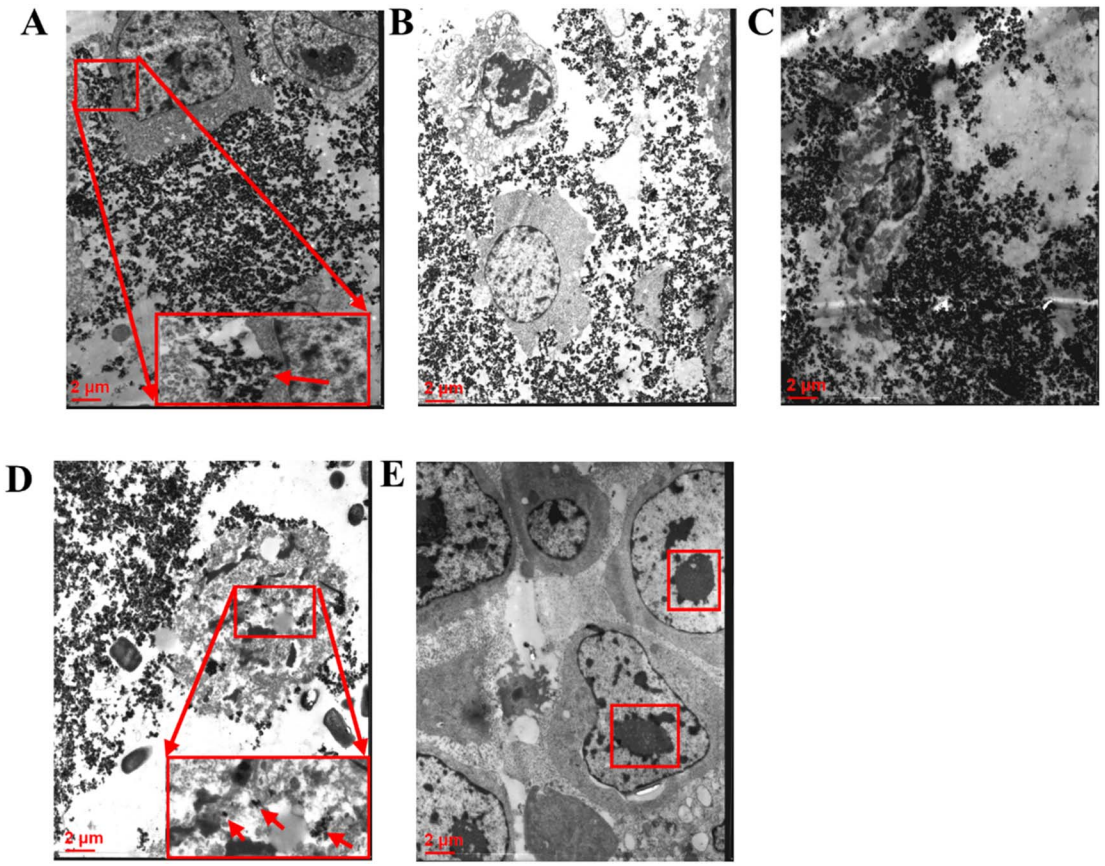

Fig. 4 Distribution of magnetic nanoparticles in tumor cell. Electron microscopy images (4000×): (A) PEI-MNPs in the cytoplasm; (B & C) large amounts of magnetic nanoparticles surrounding tumor cells; (D) damaged cells containing magnetic nanoparticles; (E) tumor cells with prominent nucleoli. Scale bar is 2 μm.

(17.97, 30.81) cm^3, C group 30.20 (24.72, 32.14) cm^3, M group 30.51 (28.71, 34.37) cm^3, MF group 29.31 (27.56, 32.23) cm^3, and MTX group 25.92 (22.77, 32.80) cm^3. Kruskal–Wallis H test was used to compare multiple independent samples, and the difference was statistically significant ($H = 69.36$, $P = 0.000$). There were significant differences in comparisons between the 47 TC, 47T, and repeated 42T groups *versus* the 42T, MFC, C, M, MF, and MTX groups ($P' < 0.0045$). Similarly, significant differences were observed when comparing the repeated 42TC group with the C, M, MF, and MTX groups ($P' < 0.0045$). See Table 1.

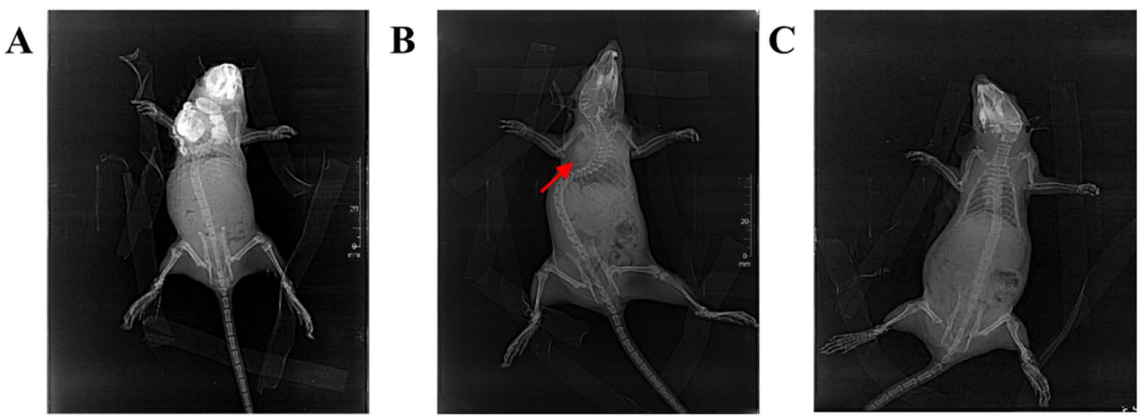

Fig. 5 X-ray photograph for different times after injection of magnetic fluid in rats. (A) X-ray photograph of one rat from the 47TC group. (B) X-ray photograph of one rat from the 47T group, showing the residual high-density shadow of the magnetic fluid indicated by the arrow. (C) X-ray photograph of one rat from the repeated 42T group.

Table 1 Changes in tumor volume in rats after treatment (cm^3)

Groups	Total cases	Tumor volume median (P_{25}, P_{75})
47TC	13	0.60 (0.04, 6.17)
47T	13	1.69 (0.32, 8.48)
Repeated 42 TC	10	7.03 (0.06, 15.52)
Repeated 42T	10	4.58 (0.16, 7.77)
42TC	10	22.34 (1.91, 29.88)
42T	10	22.96 (20.10, 27.33)
MFC	10	26.71 (17.97, 30.81)
C	10	30.20 (24.72, 32.14)
M	10	30.51 (28.71, 34.37)
MF	10	29.31 (27.56, 32.23)
MTX	10	25.92 (22.77, 32.80)

3.6. Observation for long-term survival after treatment

Six rats in normal group and 116 tumor inoculated rats were observed for 120 days. Six rats in normal group survived. The survival time of the rats in the 47 TC group was 120,00 (120.00, 120.00), in the 47T group was 120.00 (47.00, 120.00), in the Repeated 42 TC group was 90.00 (44.80, 120.00), in the repeated 42T group was 58.00 (49.00, 120.00), in the 42TC group was 44.50 (36.75, 60.50), in the 42T group was 43.00 (39.25, 47.50), in the MFC group was 43.00 (34.75, 71.25), in the C group was 39.00 (34.00, 42.50), in the M group was 40.50 (32.25, 45.00), in the MF group was 35.50 (33.00, 39.70), in the MTX group was 37.00 (32.50, 40.00). 84.60% (11/13) of the rats in the 47TC survived for 120 days, 53.80% (7/13) of the rats in the 47T survived, 50.00% (5/10) of the rats in the repeated 42TC survived, 30.00% (3/10) of the rats in the repeated 42T survived, 20.00% (2/10) of the rats in the MFC survived, and 10.00% (1/10) of the rats in the single 42TC survived. Kruskal–Wallis H test was used to compare multiple independent samples, and the difference was statistically significant ($H = 60.24$, $P = 0.000$). There were significant differences between 47TC group and 42TC, 42T, MFC, C, M, MF and MTX group ($P'' < 0.004$). There were statistically significant differences between group 47T and C, M, MF and MTX ($P'' < 0.004$). The differences between repeated 42TC group and M, MF and MTX group were statistically significant ($P'' < 0.004$). See Table 2.

3.7. IL-2, IFN-γ, IL-4 detection in peripheral blood

The peripheral blood levels of IL-2 in serum were detected, and the results showed: the 47 TC group of (38.13 ± 22.63) Pg mL^{-1}, 47T group of (41.80 ± 18.25) Pg mL^{-1}, 42TC group of (17.00 ± 4.47) Pg mL^{-1}, 42T group of (15.89 ± 7.16) Pg mL^{-1}, MFC group of (17.99 ± 4.38) Pg mL^{-1}, C group of (10.79 ± 2.88) Pg mL^{-1}, MTX group of (35.83 ± 13.51) Pg mL^{-1}, normal group of (37.06 ± 15.63) Pg mL^{-1}. The C group were statistically significantly different from the 47TC, 47T, MTX and the normal group respectively ($P < 0.05$). 42TC group and 42T group were statistically significantly different from the 47TC, 47T, and the normal group respectively ($P < 0.05$). MFC group were statistically significantly different from the 47T group ($P < 0.05$). See Fig. 6A. Thus, the IL-2 levels in the peripheral blood after treatment in the 47TC group, 47T group were higher than in the C, 42TC and 42T group, and no significant difference was found with the normal group. The peripheral blood IFN-γ levels in serum were detected, and the results showed: the 47 TC group of (58.70 ± 6.14) Pg mL^{-1}, 47T group of (59.76 ± 15.69) Pg mL^{-1}, 42TC group of (63.49 ± 5.46) Pg mL^{-1}, 42T group of (55.27 ± 12.21) Pg mL^{-1}, MFC group of (45.19 ± 10.20) Pg mL^{-1}, C group of (42.79 ± 7.40) Pg mL^{-1}, MTX group of (52.79 ± 11.78) Pg mL^{-1}, normal group of (48.00 ± 5.49) Pg mL^{-1}. The lowest level in the rats of C was statistically significantly different from the 47TC, 47T and 42TC group ($P < 0.05$). The levels in the rats of MFC were statistically significantly different from the 47T and 42 TC group ($P < 0.05$), and the normal group were significantly different from the 42TC group ($P < 0.05$). See Fig. 6B. The levels of C group were the lowest, indicating the thermotherapy/thermochemotherapy increased the levels of IFN-γ. The peripheral blood IL-4 levels in serum were detected, and the results showed: the 47TC group of (60.71 ± 16.84) Pg mL^{-1}, 47T group of (38.42 ± 7.35) Pg mL^{-1}, 42TC group of (43.04 ± 15.27) Pg mL^{-1}, 42T group of (37.90 ± 10.15) Pg mL^{-1}, MFC group of (47.67 ± 13.68) Pg mL^{-1}, C group of (86.07 ± 17.77) Pg mL^{-1}, MTX group of (38.63 ± 10.42) Pg mL^{-1}, normal group of (36.48 ± 8.23) Pg mL^{-1}. The comparison of levels was significantly different between the C group and other groups ($P < 0.05$). The levels in the rats of 47TC group were statistically significantly different from the 47T, 42T, C, MTX and the normal group ($P < 0.05$). See Fig. 6C.

Table 2 Survival number and median survival time of rats in each group (months)

Groups	Total cases	Number of survivors	Survival time median (P_{25}, P_{75})
47TC	13	11	120.00 (120.00, 120.00)
47T	13	7	120.00 (47.00, 120.00)
Repeated 42TC	10	5	90.00 (44.80, 120.00)
Repeated 42T	10	3	58.00 (49.00, 120.00)
42TC	10	1	44.50 (36.75, 60.50)
42T	10	0	43.00 (39.25, 47.50)
MFC	10	2	43.00 (34.75, 71.25)
C	10	0	39.00 (34.00, 42.50)
M	10	0	40.50 (32.25, 45.00)
MF	10	0	35.50 (33.00, 39.70)
MTX	10	0	37.00 (32.50, 40.00)
Normal	6	6	120.00 (120.00, 120.00)

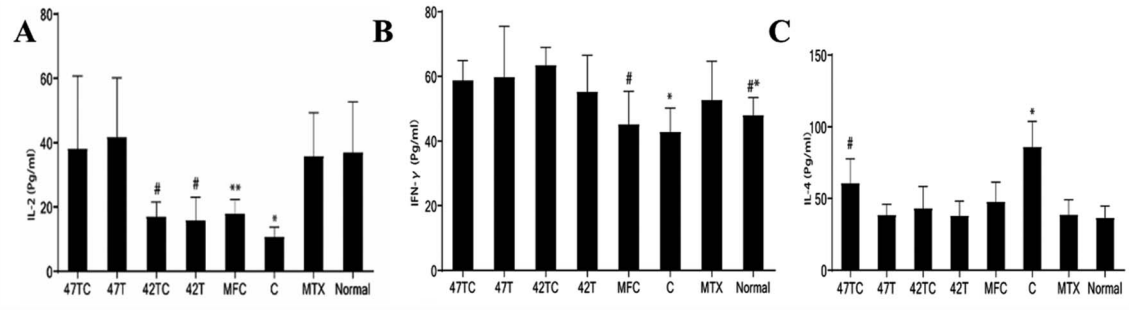

Fig. 6 IL-2, IFN-γ, IL-4 levels of rats in the peripheral blood. (A) * Compared with the 47TC, 47T, MTX, normal group, $P < 0.05$; ** compared with the 47T, $P < 0.05$; # compared with the 47TC, 47T, normal group $P < 0.05$. (B) *Compared with the 47TC, 47T, 42TC group, $P < 0.05$; #compared with the 47T, 42TC group, $P < 0.05$; #*compared with the 42TC group, $P < 0.05$. (C) *Compared with each group, $P < 0.05$; #compared with the 47T, 42T, C, MTX, Normal group, $P < 0.05$.

4. Discussion

For nano-magnetic particles, heat is generated under the action of alternating magnetic fields through two mechanisms: the rotation of the magnetic vector inside the particles, known as Néel relaxation, and the physical rotation of the particles themselves, known as Brownian relaxation.[23,24] The PEI-modified Fe_3O_4 magnetic fluids used in this experiment was covalently combined with MTX, and the particle diameter was about 10 nm under TEM, showing superparamagnetic properties. PEI modified Fe_3O_4 magnetic fluid and MTX modified magnetic fluid both have good dispersibility, are not easy to agglomerate *in vitro*, and heat up rapidly. *In vivo* experiments also found that the temperature rise is faster, which can better meet the experimental requirements. The magnetic fluid containing MTX used in this experiment can be used for magnetic hyperthermia chemotherapy, which not only has the effect of hyperthermia, but also allows the local sustained release of chemotherapy drugs to increase the local concentration of chemotherapy drugs and reduce the systemic toxic side effects.[2,19,23]

4.1. Effects of magnetic thermotherapy or thermochemotherapy on tumors

Thermotherapy is an effective method for tumor treatment. The basic physical quantity reflecting the biological effects of thermal dose is the temperature and time. When evaluating the relationship between different temperature and time with cell survival, the Arrhenius equivalent relationship of thermal biological effects is generally used. Its contents are summarized follows: for each 1 °C increase temperature above 43 °C, the treatment time should be halved to achieve the same cytotoxic effect.[25–27] This indicates that in the heating temperature and time two thermal dose factors, the temperature is more decisive. Generally, low temperature hyperthermia refers to heating the whole body or tumor tissue to 39–42 °C, and high temperature hyperthermia is heating the temperature to more than 45 °C. 42 °C is low temperature hyperthermia, 47 °C is high temperature hyperthermia. We used PEI modified magnetic fluid hyperthermia (MFH) and MTX carrying magnetic fluid thermochemotherapy for the first time to treat tumor bearing rats, and tumor was disappeared in 2 rats of the 47 TC group, 2 rats of the 47T group, and 1 rat of each of the repeated 42TC and repeated 42T groups after 14 days of thermotherapy/thermochemotherapy. The survival rate of rats in the 47 °C, 30 min thermochemotherapy group was higher than that in the 42 °C, 60 min of thermotherapy and thermochemotherapy group, suggesting that temperature is the main factor affecting the survival rate of rats. The 47TC group had the highest survival rate, with a significantly longer survival time compared to the 42TC, 42T, MFC, M, C, MF, and MTX groups, demonstrating the synergistic effect of hyperthermia and chemotherapy. Repeating hyperthermia every 72 hours is aimed at overcoming thermal tolerance. This allows repeated temperature treatments to increase the thermal sensitivity of tumors. There was no statistically significant difference in long-term survival between the repeated 42TC and repeated 42T groups compared to the 42TC and 42T groups. However, 50% of rats in the repeated 42TC group and 30% in the repeated 42T group survived long-term, while only 10% of rats in the 42TC group survived and none in the 42T group, which is related to the small sample size of this study. Some tumors of rats in the 42TC, 42T group were shrinked after treatment, but the control time to tumor was short, the tumor soon restored the original growth rate. In the 42TC group, the complete remission occurred for the tumor of 2 rats, but one died of tumor recurrence, showing that the low temperature thermochemotherapy was ineffective, possibly because the magnetic nanoparticles in the tumor margins were distributed unevenly, thus becoming the root of residual tumor recurrence. Secondly, the temperature 42 °C may be associated with the weaker killing effects on the neoplastic cells of Walker-256 breast cancer, and multiple thermotherapy/thermochemotherapy can improve the therapeutic effects.[24,28] It has been reported that the MTX in the 20–250 mg kg^{-1} can be considered for the high-dose chemotherapy.[20,29,30] We used 20 mg kg^{-1} local injection of chemotherapy drugs MTX, no death was observed within a few days in rats of MTX group, but no rats can be recovered, considering that this was due to the rapid elimination of the MTX chemotherapy drug in the body. Compared with the C group, the

slower growth of tumor in rats of MFC group may be associated with a certain inhibition to tumor by the slow release of chemotherapy drug. The recovery of 2 rats in the MFC group may be related to the dose of the chemotherapy drug. We use magnetic fluid contain 5.7 mg MTX per 1 mL, 2.5 mL average dose was injected for each rat, with the content of 14.25 mg MTX, more than 7 times higher than 2 mg of dose for each rat in the MTX group, which may be the reason for 2 recovered rats in the MFC group, but may be related to the local sustained release of chemotherapy drug which can kill the tumor, activate simultaneously the body's own immune function. In the preliminary experiment, we injected 14 mg MTX per rat into the tumor area of 4 rats (not included in this study). The rats experienced significant fecal death within 3–5 days, considering that high dose MTX chemotherapy resulted in severe gastrointestinal damage in the rats. The average injection of approximately 2.5 mL of magnetic fluid into each rat resulted in a slightly higher MTX content of 14.25 mg compared to 14 mg, indicating that the magnetic fluid used in this experiment is safe and tolerable. The current study on MFH is still more in the animal experimental phase, using xenografts tumor models, involving liver cancer, lung cancer, tongue cancer, breast cancer, prostate cancer, cervical cancer, melanoma, glioblastoma and other types, and these studies have achieved a better therapeutic effect.[2,31–34] Moreover, it has also been reported in the literature that MFH can promote the immune response, improve the effect of chemotherapy and reduce the chemotherapeutics side effects, reducing the radiation dose and improved the radiation therapeutic effect.[2,11,12,35–37] With the progress of research and development of magnetic equipment and improvement of magnetic fluid technology, in 2005, Johnnsen *et al.*[22] used the magnetic fluid encapsulated with aminosilane to conduct the world's first human MFH treatment of prostate cancer, marking the MFH application into a new stage. Currently, the treatment has been conducted in the prostate cancer, glioblastoma, liver cancer, pancreas tumors, bone tumors and a minority of metastatic carcinoma, and the studies have suggested that the targeting of magnetic fluid is better, and has achieved some therapeutic effects.[11–14] Thermochemotherapy with magnetic microspheres containing drugs is an emerging cancer treatment following the magnetically mediated tumor hyperthermia.[33] Its advantages are as follows: it can carry different chemotherapy drugs and conduct different surface modification to achieve specific thermochemotherapy effects for different tumors; it can connect the antibodies, gene *etc.*,[2,7,12,38] to the magnetic microspheres to achieve other biological functions at the same time of play a role in thermochemotherapy.

In this experiment, it was found that the magnetic nanoparticles in the small blood vessels of meninges of one rat may be the magnetic nanoparticles entering into the small blood vessels of tumor during injection of tumor and being brought into the meningeal blood vessels with the blood flow. There was no deposition of magnetic nanoparticles in the heart, liver, lung, kidney and brain tissues, which was slightly different from the negligible deposition of magnetic nanoparticles in the heart, liver and kidney reported by Chauhan *et al.*[39] Considering that this study was only examined with a 5 μm thick biopsy tissue and cannot fully understand the distribution of magnetic nanoparticles in various visceral organs, future experiments will be done for detection of iron content in various organs by plasma mass spectrometry, which will be helpful to understand the residual circumstances of the magnetic nanoparticles in each organ. In 11 rats, residues of magnetic nanoparticles were visibly present under the skin to the naked eye, and through 120 days of observation, it was found that these visible residues had no significant effect on the survival of the rats. The specific metabolic mechanisms by which subcutaneous magnetic nanoparticles are processed require further study.

4.2. The effect of magnetic hyperthermia or thermochemotherapy on the immunity of tumor bearing rats

Suzuki *et al.*[40] used a magnetic cationic liposome for the local heating treatment in mice with melanoma, the tumor of 90% mice in the treatment group disappeared completely, and through the analysis of splenocytes toxicity for the recovered mice, indicating that the tumor regression is not only induced by temperature, but also the important effects of anti-tumor immunity. The study found magnetic fluid hyperthermia can enhance immune function and resistance to the tumor growth.[34,39,41–43] Helper T cells are divided into Th1, Th2 two types, both have an important regulatory role in the cellular and humoral immunity of the body. Th1 cells mainly secrete IL-2, IFN-γ, TNF-β, *etc.*, and Th2 cells mainly secrete IL-4, IL-5, IL-10, the former can mainly mediate the cellular immunologic response, and the latter can mainly mediate the humoral immunologic response.[44] Generally believed that cellular immunity is the body's main form of anti-tumor immunity, under the normal circumstances, Th1, Th2 can be at the state of relative equilibrium, once the Th1 shifts towards Th2, the anti-tumor immunity of the body will be severely disrupted.[45,46] Thus, the function determination of Th1, Th2 can be helpful to the clinical judgment of cancer patient's immune status, prognosis, and to provide a theoretical basis for effective cancer biotherapy. In this experiment, the levels of IL-2 and IFN-γ in the C group were lower, IL-4 levels were significantly higher in the C group, suggesting that the C group rats showed shift from Th1 to Th2 and the immune function of rats was inhibited. The IL-4 levels in the 47TC were only lower than in the C group, suggesting that the high temperature thermochemotherapy can activate the cellular immune function of the body and also simultaneously activate the humoral immune function, and the specific mechanism needs further study. The IL-2 levels were higher in 47TC and the 47T group, no significant difference was found with the normal group, but higher than in the 42TC, 42T, and C group. The IFN-γ levels in 47 TC and 47T group were higher than C group after treatment, suggesting that 47 °C for 30 min high temperature thermochemotherapy and thermotherapy can increase the expression levels of Th1, thus activating the cellular immune function of the body.

5. Summary

On the whole, the magnetic nanoparticles were evenly distributed in the center area of the tumor tissues, the unevenly distributed at the tumor edge. Magnetic nanoparticles entered cytoplasm, the wider distribution around the tumor cells. MTX-MNPs injected into tumor tissue can induce complete tumor remission and long-term survival in some tumor-bearing rats and activate the immune function of the body. MTX-MNPs have no visceral organs residue and are safe and tolerable, which provides a certain basis for future research. Combining magnetic nanomaterials with newly discovered tumor therapeutic targets is an inevitable trend in future research, poised to profoundly impact tumor treatment. Research on the absorption rate and release behavior of drug molecules within magnetic nanoparticles is a key direction in the development of controlled drug release technologies. The future of drug release technology lies in nano drugs that are both highly safe and capable of intelligent drug release. With advances in nanomaterials and biotechnology, targeted nano drugs are expected to exhibit superior anti-tumor activity with fewer toxic side effects, thereby laying a solid foundation for clinical applications.

Data availability

All data used in this study are available upon reasonable request. The data are stored in the data repository of the Department of Thoracic Oncology at the Affiliated Hospital of Guizhou Medical University and the Affiliated Cancer Hospital of Guizhou Medical University. For access to the data, please contact Weiwei Ouyang (email: ouyangww103173@163.com).

Author contributions

WWOY designed the study. LH, XZ, JQZ, WKL, YHF, FPG and JZ performed the experiments. Data were collated by LH, XZ and FPG. JZ performed pathology smears and data collection. The results of data were discussed by JTT, FPG, WWOY and JTT, LH, XZ and JQZ prepared the figures. LH, XZ, JZ, JTT and WWOY wrote the first draft of the manuscript. All authors read and approved the final version of the manuscript.

Conflicts of interest

The authors declare no competing interests.

Acknowledgements

This study was funded by Key Program for Science and Technology of Guizhou Province [Grant No. ZK(2021)012].

Notes and references

1 J. Jose, R. Kumar, S. Harilal, G. E. Mathew, D. G. T. Parambi, A. Prabhu, M. S. Uddin, L. Aleya, H. Kim and B. Mathew, Magnetic nanoparticles for hyperthermia in cancer treatment: an emerging tool, *Environ. Sci. Pollut. Res. Int.*, 2020, **27**, 19214–19225.

2 A. Farzin, S. A. Etesami, J. Quint, A. Memic and A. Tamayol, Magnetic Nanoparticles in Cancer Therapy and Diagnosi, *Adv. Healthcare Mater.*, 2020, **9**, e1901058.

3 A. Ali, T. Shah, R. Ullah, P. Zhou, M. Guo, M. Ovais, Z. Tan and Y. Rui, Review on Recent Progress in Magnetic Nanoparticles: Synthesis, Characterization, and Diverse Applications, *Front. Chem.*, 2021, **9**, 629054.

4 N. A. Brusentsov, V. A. Polianskiy, A. V. Zhukov, M. V. Gulyaev, M. P. Nikitin, P. I. Nikitin, T. N. Brusentsova, V. D. Kuznetsov, O. A. Bocharova and A. Y. Baryshnikov, Combined Photodynamic Thermochemotherapy of Glial Tumors Controlled by MRI and Electronic Sensor, *Solid State Phenom.*, 2015, **233–234**, 757–760.

5 M. Li, L. Deng, J. Li, W. Yuan, X. Gao, J. Ni, H. Jiang, J. Zeng, J. Ren and P. Wang, Actively Targeted Magnetothermally Responsive Nanocarriers/Doxorubicin for Thermochemotherapy of Hepatoma, *ACS Appl. Mater. Interfaces*, 2018, **10**, 41107–41117.

6 K. Hayashi, Y. Sato, W. Sakamoto and T. Yogo, Theranostic Nanoparticles for MRI-Guided Thermochemotherapy: "Tight" Clustering of Magnetic Nanoparticles Boosts Relaxivity and Heat-Generation Power, *ACS Biomater. Sci. Eng.*, 2017, **3**, 95–105.

7 Y. Zeng, Z. Yang, H. Li, Y. Hao, C. Liu, L. Zhu, J. Liu, B. Lu and R. Li, Multifunctional Nanographene Oxide for Targeted Gene-Mediated Thermochemotherapy of Drug-resistant Tumour, *Sci. Rep.*, 2017, **7**, 43506.

8 W. Y. Tak, S. M. Lin, Y. Wang, J. Zheng, A. Vecchione, S. Y. Park, M. H. Chen, S. Wong, R. Xu, C. Y. Peng, Y. Y. Chiou, G. T. Huang, J. Cai, B. J. J. Abdullah, J. S. Lee, J. Y. Lee, J. Y. Choi, J. Gopez-Cervantes, M. Sherman, R. S. Finn, M. Omata, M. O'Neal, L. Makris, N. Borys, R. Poon and R. Lencioni, Phase III HEAT Study Adding Lyso-Thermosensitive Liposomal Doxorubicin to Radiofrequency Ablation in Patients with Unresectable Hepatocellular Carcinoma Lesions, *Clin. Cancer Res.*, 2018, **24**, 73–83.

9 N. Elahi and M. Rizwan, Progress and prospects of magnetic iron oxide nanoparticles in biomedical applications: A review, *Artif. Organs*, 2021, **45**, 1272–1299.

10 M. Overchuk and G. Zheng, Overcoming obstacles in the tumor microenvironment: Recent advancements in nanoparticle delivery for cancer theranostics, *Biomaterials*, 2018, **156**, 217–237.

11 D. Rivera, A. J. Schupper, A. Bouras, M. Anastasiadou, L. Kleinberg, D. L. Kraitchman, A. Attaluri, R. Ivkov and C. G. Hadjipanayis, Neurosurgical Applications of Magnetic Hyperthermia Therapy, *Neurosurg. Clin. N. Am.*, 2023, **34**, 269–283.

12 H. Zhang, S. Li, F. Chen, X. Ma and M. Liu, The therapeutic effect of PEI-Fe_3O_4/pYr-ads-8-5HRE-cfosp-IFNG albumin nanospheres combined with magnetic fluid hyperthermia on hepatoma, *Front. Oncol.*, 2023, **13**, 1080519.

13 P. Chandrasekharan, Z. W. Tay, D. Hensley, X. Y. Zhou, B. K. Fung, C. Colson, Y. Lu, B. D. Fellows, Q. Huynh, C. Saayujya, E. Yu, R. Orendorff, B. Zheng, P. Goodwill, C. Rinaldi and S. Conolly, Using magnetic particle imaging systems to localize and guide magnetic hyperthermia treatment: tracers, hardware, and future medical applications, *Theranostics*, 2020, **10**, 2965–2981.

14 F. Vergnaud, X. Kesse, A. Jacobs, F. Perton, S. Begin-Colin, D. Mertz, S. Descamps, C. Vichery and J. M. Nedelec, Magnetic bioactive glass nano-heterostructures: a deeper insight into magnetic hyperthermia properties in the scope of bone cancer treatment, *Biomater. Sci.*, 2022, **10**, 3993–4007.

15 W. Yang, J. C. Lee, M. H. Chen, Z. Y. Zhang, X. M. Bai, S. S. Yin, K. Cao, S. Wang, W. Wu and K. Yan, Thermosensitive liposomal doxorubicin plus radiofrequency ablation increased tumor destruction and improved survival in patients with medium and large hepatocellular carcinoma: A randomized, double-blinded, dummy-controlled clinical trial in a single center, *J. Cancer Res. Ther.*, 2019, **15**, 773–783.

16 B. J. Wood, R. T. Poon, J. K. Locklin, M. R. Dreher, K. K. Ng, M. Eugeni, G. Seidel, S. Dromi, Z. Neeman, M. Kolf, C. D. Black, R. Prabhakar and S. K. Libutti, Phase I study of heat-deployed liposomal doxorubicin during radiofrequency ablation for hepatic malignancies, *J. Vasc. Interv. Radiol.*, 2012, **23**, 248–255.

17 M. Stapf, N. Pömpner, U. Teichgräber and I. Hilger, Heterogeneous response of different tumor cell lines to methotrexate-coupled nanoparticles in presence of hyperthermia, *Int. J. Nanomed.*, 2016, **11**, 485–500.

18 Q. Li, Y. Chen, X. Zhou, D. Chen, Y. Li, J. Yang and X. Zhu, Hyaluronic Acid-Methotrexate Conjugates Coated Magnetic Polydopamine Nanoparticles for Multimodal Imaging-Guided Multistage Targeted Chemo-Photothermal Therapy, *Mol. Pharm.*, 2018, **15**, 4049–4062.

19 X. Li, W. Li, M. Wang and Z. Liao, Magnetic nanoparticles for cancer theranostics: Advances and prospects, *J. Controlled Release*, 2021, **335**, 437–448.

20 E. H. M. Hassanein, H. S. Althagafy, A. M. Atwa, M. R. Kozman, M. I. Kotb El-Sayed and A. A. Soubh, Taurine attenuated methotrexate-induced intestinal injury by regulating NF-κB/iNOS and Keap1/Nrf2/HO-1 signals, *Life Sci.*, 2022, **311**, 121180.

21 I. Hilger, W. Andrä, R. Hergt, R. Hiergeist, H. Schubert and W. A. Kaiser, Electromagnetic heating of breast tumors in interventional radiology: in vitro and in vivo studies in human cadavers and mice, *Radiology*, 2001, **218**, 570–575.

22 M. Johannsen, U. Gneveckow, L. Eckelt, A. Feussner, N. Waldöfner, R. Scholz, S. Deger, P. Wust, S. A. Loening and A. Jordan, Clinical hyperthermia of prostate cancer using magnetic nanoparticles: presentation of a new interstitial technique, *Int. J. Hyperthermia*, 2005, **21**, 637–647.

23 D. Rahban, M. Doostan and A. Salimi, Cancer Therapy; Prospects for Application of Nanoparticles for Magnetic-Based Hyperthermia, *Cancer Invest.*, 2020, **38**, 507–521.

24 M. T. Luiz, J. A. P. Dutra, J. S. R. Viegas, J. T. C. de Araújo, A. G. Tavares Junior and M. Chorilli, Hybrid Magnetic Lipid-Based Nanoparticles for Cancer Therapy, *Pharmaceutics*, 2023, **15**, 751.

25 P. X. E. Mouratidis, I. Rivens, J. Civale, R. Symonds-Tayler and G. Ter Haar, Relationship between thermal dose and cell death for "rapid" ablative and "slow" hyperthermic heating, *Int. J. Hyperthermia*, 2019, **36**, 229–243.

26 E. Happonen, K. Tamarov, M. V. Martikainen, K. Ketola, M. Roponen, V. P. Lehto and W. Xu, Thermal dose as a universal tool to evaluate nanoparticle-induced photothermal therapy, *Int. J. Pharm.*, 2020, **587**, 119657.

27 G. C. Van Rhoon, M. Franckena and T. L. M. Ten Hagen, A moderate thermal dose is sufficient for effective free and TSL based thermochemotherapy, *Adv. Drug Delivery Rev.*, 2020, **163–164**, 145–156.

28 D. Rivera, A. J. Schupper, A. Bouras, M. Anastasiadou, L. Kleinberg, D. L. Kraitchman, A. Attaluri, R. Ivkov and C. G. Hadjipanayis, Neurosurgical Applications of Magnetic Hyperthermia Therapy, *Neurosurg. Clin. N. Am.*, 2023, **34**, 269–283.

29 A. C. Famurewa, A. M. Folawiyo, M. A. Epete, E. C. Igwe, P. I. Okike and E. K. Maduagwuna, Abrogation of Hepatic Damage Induced by Anticancer Drug Methotrexate by Zobo (Hibiscus sabdariffa extract) Supplementation via Targeting Oxidative Hepatotoxicity in Rats, *J. Diet. Suppl.*, 2019, **16**, 318–330.

30 J. E. Fardell, J. Vardy, W. Logge and I. Johnston, Single high dose treatment with methotrexate causes long-lasting cognitive dysfunction in laboratory rodents, *Pharmacol., Biochem. Behav.*, 2010, **97**, 333–339.

31 J. Palzer, L. Eckstein, I. Slabu, O. Reisen, U. P. Neumann and A. A. Roeth, Iron Oxide Nanoparticle-Based Hyperthermia as a Treatment Option in Various Gastrointestinal Malignancies, *Nanomaterials*, 2021, **11**, 3013.

32 S. V. Spirou, M. Basini, A. Lascialfari, C. Sangregorio and C. Innocenti, Magnetic Hyperthermia and Radiation Therapy: Radiobiological Principles and Current Practice, *Nanomaterials*, 2018, **8**, 401.

33 P. Das, M. Colombo and D. Prosperi, Recent advances in magnetic fluid hyperthermia for cancer therapy, *Colloids Surf., B*, 2019, **174**, 42–55.

34 M. Chang, Z. Hou, M. Wang, C. Li and J. Lin, Recent Advances in Hyperthermia Therapy-Based Synergistic Immunotherapy, *Adv. Mater.*, 2021, **33**, e2004788.

35 M. H. Chan, C. H. Li, Y. C. Chang and M. Hsiao, Iron-Based Ceramic Composite Nanomaterials for Magnetic Fluid Hyperthermia and Drug Delivery, *Pharmaceutics*, 2022, **14**, 2584.

36 Q. Qin, Y. Zhou, P. Li, Y. Liu, R. Deng, R. Tang, N. Wu, L. Wan, M. Ye, H. Zhou and Z. Wang, Phase-transition nanodroplets with immunomodulatory capabilities for potentiating mild magnetic hyperthermia to inhibit tumour proliferation and metastasis, *J. Nanobiotechnol.*, 2023, **21**, 131.

37 A. L. Oei, H. P. Kok, S. B. Oei, M. R. Horsman, L. J. A. Stalpers, N. A. P. Franken and J. Crezee, Molecular

and biological rationale of hyperthermia as radio- and chemosensitizer, *Adv. Drug. Deliv. Rev.*, 2020, **163–164**, 84–97.

38 T. S. Anilkumar, K. T. Shalumon and J. P. Chen, Applications of Magnetic Liposomes in Cancer Therapies, *Curr. Pharm. Des.*, 2019, **25**, 1490–1504.

39 A. Chauhan, S. Midha, R. Kumar, R. Meena, P. Singh, S. K. Jha and B. K. Kuanr, Rapid tumor inhibition via magnetic hyperthermia regulated by caspase 3 with time-dependent clearance of iron oxide nanoparticles, *Biomater. Sci.*, 2021, **9**, 2972–2990.

40 M. Suzuki, M. Shinkai, H. Honda and T. Kobayashi, Anticancer effect and immune induction by hyperthermia of malignant melanoma using magnetite cationic liposomes, *Melanoma Res.*, 2003, **13**, 129–135.

41 T. Li, Z. Hu, F. Song, C. Wu, Q. Miao, Z. Wang, W. Feng, J. Guo and Y. Chen, Photonic Hyperthermia Synergizes with Immune-Activators to Augment Tumor-Localized Immunotherapy, *Small Methods*, 2023, **7**, e2300116.

42 J. Pan, P. Hu, Y. Guo, J. Hao, D. Ni, Y. Xu, Q. Bao, H. Yao, C. Wei, Q. Wu and J. Shi, Combined Magnetic Hyperthermia and Immune Therapy for Primary and Metastatic Tumor Treatments, *ACS Nano*, 2020, **14**, 1033–1044.

43 D. Cui, Y. Han, Z. Li, H. Song, K. Wang, R. He, B. Liu, H. Liu, C. Bao, P. Huang, J. Ruan, F. Gao, H. Yang, H. S. Cho, Q. Ren and D. Shi, Fluorescent Magnetic Nanoprobes for in vivo Targeted Imaging and Hyperthermia Therapy of Prostate Cancer, *Nano Biomed. Eng.*, 2009, **1**, 61–74.

44 E. Dai, Z. Zhu, S. Wahed, Z. Qu, W. J. Storkus and Z. S. Guo, Epigenetic modulation of antitumor immunity for improved cancer immunotherapy, *Mol. Cancer*, 2021, **20**, 171.

45 H. Qin, Y. Lu, L. Du, J. Shi, H. Yin, B. Jiang, W. Chen, W. Diao, M. Ding, W. Cao, X. Qiu, X. Zhao and H. Guo, Pan-cancer analysis identifies LMNB1 as a target to redress Th1/Th2 imbalance and enhance PARP inhibitor response in human cancers, *Cancer Cell Int.*, 2022, **22**, 101.

46 Y. Fu, Q. Lin, Z. Zhang and L. Zhang, Therapeutic strategies for the costimulatory molecule OX40 in T-cell-mediated immunity, *Acta Pharm. Sin. B*, 2020, **10**, 414–433.